Mechanisms and Kinetics of Boron Removal from Silicon by Humidified Hydrogen

Jafar Safarian[1], Kai Tang[1], Jan Erik Olsen[1], Stefan Andersson[1], Gabriella Tranell[2], Kjetil Hildal[3]

[1] SINTEF Materials and Chemistry, Alfred Getz Vei 2, N-7465 Trondheim, Norway

[2] Norwegian University of Science and Technology (NTNU), N-7491, Trondheim, Norway

[3] ELKEM Technology, N-4675, Kristiansand, Norway

Keywords: Silicon, Refining, Boron, Gas, Steam, Kinetics, Mechanism

Abstract

The removal of boron from silicon by top blowing of humidified hydrogen has been studied in the present work through experimental work, thermodynamic calculations, computational fluid dynamic modeling, and quantum chemistry calculations. The effect of process parameters; temperature, lance diameter, lance distance from the melt surface, gas flow rate, and crucible material on the kinetics of boron removal were studied. It has been shown that the rate of boron removal is decreased with increasing temperature due to the competitive reactions between silicon and oxygen as well as boron and oxygen, which can be confirmed with the increases of p_{SiO}/p_{HBO} in the system. The rate of boron removal is increased with increasing the gas flow rate due mainly to the better supply and transport of the gas over the melt surface, as confirmed by the CFD modeling. Moreover, the rate of boron removal in alumina crucible is the highest followed by that in quartz and graphite crucibles, respectively. Faster B removal in quartz crucible than that in graphite crucible can be attributed to more oxygen dissolves in silicon melts. The fastest boron removal in alumina crucible is attributed

to the additional boron gasification through aluminum borate ($AlBO_2$) formation on the melt surface. Thermodynamic properties of the $AlBO_2$ species have thus been revised by quantum chemistry calculations, which were more accurate to describe the formation of gaseous $AlBO_2$ than those in the JANAF Thermochemical Tables.

The main chemical reactions for boron gasification from silicon melts are proposed as:

In graphite, quartz and alumina crucible: $\underline{B} + \underline{H} + \underline{O} = HBO\ (g)$

In alumina crucible: $\underline{Al} + \underline{B} + \underline{O} = AlBO_2\ (g)$

Based on the obtained results, it has been proposed that boron removal from silicon melt by humidified hydrogen is controlled both by the chemical reaction for boron gasification and mass transport in the adjacent gas phase.

I. Introduction

Silicon is still the dominant semiconductor material used in the photovoltaic (PV) industry. Solar grade silicon (SoG-Si) is a high purity material with above 99.9999 %Si, which can be produced through chemical and metallurgical routes. The purity of the silicon produced by the chemical processes is usually higher than that produced through metallurgical processes; and often above that required for photovoltaic applications. The most common route to produce SoG-Si from Metallurgical Grade Silicon (MG-Si) is still based around so-called the Siemens technology which includes gasification, distillation and re-deposition of silicon via trichlorosilane, a very energy intensive method which also generates significant amounts of chemical waste. [1] Hence, more cost effective metallurgical processes for making solar grade silicon – with less environmental impact – have been studied and developed in the recent years due to the rapid PV market growth. Boron (B) and phosphorus (P) are the two crucial impurity elements that are most difficult to be removed from silicon, since they cannot be effectively separated by directional solidification, a key process step for removing many

impurities such as Fe, Ti, Al, Ca, Mg, *etc.*. The removal of B and P requires the dedicated refining processes and has been the motivation of many purification process studies. In addition to boron slag refining technology, which is currently applied industrially by ELKEM Solar AS, the removal of B can be performed through the treatment of liquid silicon by oxidative plasma or other gas refining techniques. In these processes, the dissolved B in molten silicon is gasified through the formation of volatile B-containing compounds.

The removal of boron by different reactive gases, such as O_2[2,3], H_2[4,5], CO_2[3], and H_2O[6,7,8,9,10,11,12], has been studied through several research groups. It has been observed that the application of the H_2-O_2 gas mixtures in plasma refining is more effective in terms of the kinetics of B removal compared to the single H_2, O_2, CO_2 gases[13,14]. Recent experimental studies on B removal by H_2O-containing gases in top gas blowing technique has shown the possibility of B removal by this technique to extreme low levels, below 1 ppmw[4,12,15]. The presence of hydrogen in the refining gas causes the formation of H-B-O volatile species such as the HBO gaseous species on the melt surface, which are more volatile than the H-B and B-O species [12]. The effects of process parameters such as gas composition, gas flow rate, lance parameters and temperature on the B removal kinetics has been studied recently. It has been observed that the rate of B removal is decreased with increasing temperature [4,12,15]. Moreover, the rate of B removal is higher using the binary H_2-H_2O gas mixtures than other types of gas mixtures, such as humidified argon and nitrogen [12], as well as the Ar-H_2-H_2O gas mixtures [4]. Moreover, the rate of B removal is increased with increasing H_2O content of the gas mixture[16], as long as a stable passive oxide layer over the melt surface does not formed through silicon oxidation to SiO_2[12]. It has also been observed that the rate of B removal from silicon is increased with increasing gas flow rate. It has thus been proposed that the kinetics of B removal is controlled by the mass transport in the gas phase [15].

The mechanism of HBO formation during silicon refining by H_2O containing gases is still not well-known. Khattak *et al*.[7] proposed that the removal of dissolved B in silicon at the melt surface can occur through its reaction with H_2 gas and the simultaneously formed SiO gas on the surface, which yields HBO gas and Si. Based on our previous experimental observations, however, we proposed[12] that the removal of B from silicon by humidified hydrogen may occur through the reaction:

$$\underline{B}+\underline{H}+ H_2O\ (g) = HBO\ (g) + H_2\ (g) \quad (1)$$

Reaction (1) occurs at the gas-liquid interface, and the dissolved hydrogen at interface is provided in the melt due to its significant solubility in silicon.[12] Based on our recent publication, [12] hydrogen existence in the refining gas is crucially important for B removal and there is significant dissolved hydrogen in the system for the chemical reaction (1). It was experimentally shown that the kinetics of B removal by H_2-H_2O gas is much higher than that by Ar-H_2O and N_2-H_2O under similar refining conditions. This indicates that B removal through its direct reaction by H_2O ($2H_2O+2B=2HBO+H_2$) is not favourable as discussed previously. [12] The mechanisms of B removal from silicon melts by the top gas blowing using humidified hydrogen have been studied in the present work. The equilibrium relations of the system are first studied to obtain a fundamental understanding of species present in the refining Si-B melt by humidified hydrogen.

II. Thermodynamics of Si-B-H-O system

Gibbs phase rule can be used to study the number of phases in the Si-B-H-O system:

$$F+P=C+2-R \quad (2)$$

where *F* denotes the number of degrees of freedom, *P* is the number of phases, *C* is the number of components, and *R* is the number of independent restrictions. Under constant pressure and temperature (R=2), for the present Si-B-O-H system, at most 4 phases can coexist: a gas phase and three condensed phases. For three component sub-systems, the faces of the illustrated sketch for Si-B-H-O system in Fig. 1, there are at most three phases that coexist. For ternary sub-systems, there is always a gas phase in equilibrium with the condensed phases. The most important compounds between each two components in Si-B-H-O system are shown on the edges of the pyramid in Fig. 1. Inspecting the databases of HSC Chemistry 7 and FactSage 6.4 Software, no three component chemical compounds in the Si-B-H and Si-B-O systems were found. It is worth noting that there is no intermediate compound between SiO_2 and B_2O_3 in their binary system [17]. However, there are many three-component gas compounds in the Si-O-H and H-B-O systems such as SiOOH, SiH_2O_3, HBO, HBO_2, HBOH, *etc*. Consequently, no four-component chemical compound was found in the Si-B-H-O system.

Using FactSage commercial software package and employing the database for solar grade silicon developed at SINTEF [18], the equilibrium compositions under fixed liquid compositions in the system at constant temperature and pressure (*R=3*) were studied. According to the Gibbs phase rule, a gas and two condensed phases coexist. The calculations reveal that solid SiO_2 is a stable phase for a wide range of H_2-H_2O mixtures over the pure silicon melts. The stable gaseous species coexist with the silicon melts with different B concentrations are shown in Fig. 2. In the equilibrium calculations, a 400 g silicon melt in contact with a H_2-3vol%H_2O gas at 1430°C was considered. This figure indicates that the most dominant gas species are H_2, SiO, H, H_2O, and Si_2O_2. Moreover, the partial pressures of B containing gas species are increased with the increase of B concentration in the Si-B melts.

More than 99.7 % of B in the gas phase appears as HBO species for the B concentrations up to 50 ppmw. Silicon in the gas phase is mainly in the form of SiO, being more than 99.8%.

III. Experimental procedure

The removal of boron from silicon melt by humidified hydrogen was studied by the top gas blowing in an induction furnace. The experimental set up is schematically shown in Fig. 3. The refining experiments were carried out using 400 g electronic grade silicon (EG-Si) melt doped to 10-25 ppmw of boron in the graphite crucible with 75mm inside and 85mm outside diameter. A set of experiments were also carried out in high purity quartz and alumina crucibles with 60mm inside diameters, keeping the surface to volume ratio of the melt as same as the experiments in graphite crucible. The gas mixtures were blown to the surface of silicon melts using the quartz lances with 2mm and 4 mm inside diameters. The measured effects of gas flow rate, temperature, lance diameter, lance distance from the melt surface on the kinetics of B-removal were compared to the previous works [4,12,15]. The effect of crucible material on the kinetics of B removal from the silicon melt was also studied. The experimental details are listed in Table I. Sampling from the melt was done during the refining experiments and the samples were subsequently analysed by high resolution Inductively Coupled Plasma Mass Spectrometry (ICP-MS). The moisture content of hydrogen gas was fixed to 3vol%H_2O for all the experiments provided by a gas humidifier (Fig. 3). A top window on the furnace allowed observing the surface of the melt during the refining experiments and investigating the formation of any passive oxide layer on the melt.

IV. Results

Three parallels of each taken sample of the melt were analysed and then averages were considered as the representative results. The effect of changing process conditions on B removal rate are described as follows.

A. Lance and gas blowing parameters

Figure 4 shows the effect of gas flow rate change on the rate of B removal from silicon. The rate of B removal is significantly increased with increasing the gas flow rate for the both lances with inner diameters. Moreover, removal of B is continued to decrease within the applied refining times for all the experiments; meaning that B can be removed to significantly low levels. Changing the inner diameters of lances from 2mm and 4mm results in reduction of the velocities of refining gases. The data in Figure 4 show that the rate of B removal is higher for higher gas velocity (smaller lance diameter) when the gas supply rate was at 1.5 NL/min, whereas the B removal rates were not significantly different for gas flow rates at 0.5 and 3.0 NL/min, respectively. Obviously, the effect of gas flow rate (gas supply) on B removal is more important than the velocity of gas for the kinetics of B removal.

The effect of changing the distance of the lance from the melt surface on the rate of B removal is shown in Fig.5. The rate of B removal reaches the lowest value when the lance tip was very close to the melt surface. However, there is no significant difference between the experiments with 3 cm and 5 cm distance of the lance from the melt surface. This indicates that the distance of the lance to the melt surface has an optimum value(s). Moreover, the distance of the lance to melt surface does not play the key role on the kinetics of B removal.

In the remain experiments in the present work, the distance of the lance to the melt was kept at 3 cm, which is a proper distance with regard to the results in Fig. 5.

B. Temperature and crucible material

Figure 6 shows the effect of temperature on the B removal rate for the fixed gas flow rates and lance sizes. Obviously, removal of B was slower at higher temperatures for the given refining conditions. This is in accordance with our previous observations.[12] and those reported by E. Nordstrand and M. Tangstad for three experimental temperatures (1500, 1550, 1600 ^{0}C).[4] Figure 6 shows that the differences between the extents of B removal at two temperatures for given experimental conditions are almost similar.

Influence of the crucible material on the rate of B removal is illustrated in Fig. 7. Some data presented in Fig. 6 are superimposed in Fig. 7 for the sake of comparison. Figure 7 shows again that the rate of B removal in quartz crucible at higher temperature is also slower than at lower temperature, although the extents of B removal after one hour are similar. This figure also shows that the rate of B removal from silicon in Al_2O_3 crucible is better than that in SiO_2 crucible, whereas the rate of B removal in graphite crucibles is the slowest. The difference of B removal rate is significant: while the B removal in alumina crucible after one hour refining is around 90%, only 50% of B removed in graphite crucible for a given refining temperature. It is worth noting that no oxide layer formation was observed on the melt surface for all types of crucibles.

C. Condensate formation

Significant amounts of a fine and very light brownish condensate was found after the refining experiments on the furnace chamber walls as well as on the lance surface. The amount of the

condensate increases with the increase of gas flow rates and temperatures. This clearly indicates that the higher rates of silicon oxidation to SiO gas by H_2O and deposition of SiO_2 from the gas on colder surfaces through SiO oxidation by the unreacted H_2O gas. This is in agreement with our previous study for the liquid silicon oxidation [19]. Although the formation of SiO_2 on the melt surface is thermodynamically possible at the process temperatures as mentioned in section II, no oxide layer resulting from a passive oxidation scheme was observed on the surface during refining for almost all the experiments, except experiment 3 after 60 minute gas blowing. It is worth noting that the produced condensate in the Exp. 3 was collected from the furnace chamber and its chemical composition was measured by ICP-MS. It was found that the condensate contains around 492 ppmw and the rest of the condensate was only SiO_2 as only elemental Si was detected. This shows condensation of the gassified B through oxidation of HBO to B_2O_3 which takes place simultaneously with SiO gas oxidation to SiO_2. The oxidizing agent in the system is the unreacted H_2O in the system.

V. Discussion

The overall mass transport coefficients for B transfer from the melt to the gas phase were determined based on the experimental results. The equilibrium calculations and computational fluid dynamic (CFD) simulation of the refining system were thus employed in order to explain the observed experimental results for B mass transport to the gas phase and also study the mechanisms involved in B removal.

A. Kinetics of B removal and the gas blowing characteristics

Considering a first order reaction for B removal from silicon[12], the total mass transport coefficient of B to the gas phase, k_B, may be calculated as:

$$k_B = \frac{ln(CB,i/CB,t)}{(A/V).t} \quad (3)$$

where $C_{B,t}$ is the concentration of B at refining time *t*, and $C_{B,i}$ is the initial concentration of B in the melt. Parameter *A* is the gas-liquid interfacial area and *V* is the volume of the melt. Fig. 8 shows the calculated k_B values for top gas blowing using a 2 mm lance at 1430°C. The related experimental data for B concentration changes were given in Fig. 4. There is a good linear relationship between $ln\ (C_{B,i}/\ C_{B,t})$ and $(A/V).t$ in the whole refining period, confirming the first order assumption for B removal kinetics. This is also in agreement with the literature [3,4,12]. The calculated mass transfer coefficients for all the experiments are summarized in Table I.

Fig. 9 shows all the calculated mass transfer coefficients against the applied gas flow rates for the experiments carried out in graphite crucible. It is observed that there is a linear relationship between the two parameters:

$$k_B = 2.88\times10^{-5}\, Q_g \quad [m/s] \quad (4)$$

The linear relationship between the k_B and Q_g indicates that the mass transport of the reaction components in the gas phase is of great important for the process kinetics. Fig. 9 also compares the present experimental results with the results reported by Sortland and Tangstad [15]. They used a H_2-4.5%H_2O gas mixture to refine 200 g silicon melt at 1500 °C. They used a 2 mm lance positioned 5 cm above the melt. Obviously, the both studies show similar effect of the gas flow rate on the boron removal kinetics.

CFD simulations were carried out in order to study the effect of gas flow rate. First a multiphase simulation was run to check the influence of deformation of metal surface

(formation of dimple).No significant deformation was observed. Then a series of simulations with flat surfaces was run for a case with a 2 mm lance opening positioned with the lance tip 3 cm above the metal surface, various flow rates and process conditions similar to some of the experiments in Fig. 4. Figures 10-a and 10-b show the change of the gas flow rate on the gas velocity magnitude. The gas velocity extend further out along the metal surface as the flow rate increases. This indicates that the mass transfer in the gas should increase with increasing the gas flow rate. The relationship between the average radial velocities of gas above the melt surface as a function of gas flow rate is shown in Fig. 11. This demonstrates clearly that higher mass transfer in gas phase is achieved by increasing the gas flow rate. Although the CFD simulation results for different lance diameters (Fig. 11) show that higher radial velocity is obtained for smaller lance diameter, it is hard to conclude the effect of lance size based on the present experimental results. However, both experiments and CFD modelling reveal that the changes in the gas flow rate is more affective on the kinetics of B removal than changing the velocity of the blowing gas through changing the lance size.

The effect of the lance tip distance from the melt surface on the gas phase velocity was also studied by CFD modelling for given refining conditions. It was found that the velocity extend further out along the metal surface if the lance is positioned further away from the metal surface. Obviously, the effect of lance position on the gas velocity is increased as also seen through comparing Figs. 10-a and 10-c. Fig. 12 shows the calculated average radial velocities for different lance positions from the melt surface. The average radial velocity increases significantly from flow rates up to 3 Nl/min. Further increasing the gas flow rate has little influence on the average radial velocity. This may be the reason of observing very close B removal rates under similar refining conditions with positioning the lance in 3 cm and 5 cm from the melt surface (Fig.5).

B. Effects of crucible material and boron gasification

The observed effects of crucible material and temperature on the rate of B removal can be discussed by studying the chemical reactions in the system. A mechanism for B removal by humidified gases through chemical reaction (1) was previously proposed as mentioned in section I. Based on the principles of heterogeneous reactions; we may consider the conversion of B to HBO gas on the surface of silicon melt through a combination of the following reactions:

$$H_2\,(g) = H_2^{\,ads.} \quad (5)$$

$$H_2^{\,ads.} = 2\,[H]^{ads.} \quad (6)$$

$$[H]^{ads.} = \underline{H} \quad (7)$$

$$H_2O\,(g) = [H_2O]^{ads.} \quad (8)$$

$$[H_2O]^{ads.} = 2\,[H]^{ads.} + [O]^{ads.} \quad (9)$$

$$[O]^{ads.} = \underline{O} \quad (10)$$

$$[H_2O]^{ads.} = [OH]^{ads.} + [H]^{ads.} \quad (11)$$

$$\underline{B} + \underline{H}\ (\text{or } [H]^{ads.}) = BH\,(g) \quad (12)$$

$$BH\,(g) + \underline{O}\ (\text{or } [O]^{ads.}) = HBO\,(g) \quad (13)$$

$$\underline{B} + [OH]^{ads.} = HBO\,(g) \quad (14)$$

$$\underline{B} + [H_2O]^{ads.} = HBO\,(g) + \underline{H} \quad (15)$$

$$\underline{B} + \underline{H} + \underline{O} = HBO\,(g) \quad (16)$$

where the adsorbed species on the melt surface are denoted by $^{ads.}$ in the above reactions. Chemical reactions (5), (6) and (7) are not rate limiting for the B removal, since there is always an excess supply of the refining gas with 97% H_2 and the hydrogen level in the melt is hence always at saturation levels [12]. Significant SiO gas formation and further oxidation to SiO_2, indicate that the chemical reaction (8) occurs very fast in the system, so that the adsorbed H_2O reacts rapidly with Si at the melt surface. Dissociation of the adsorbed H_2O to OH and O and further dissolution of oxygen, reactions (10) and (11), can be either slow or fast in the system, is not easy to extract from the current experimental results. It is worth noting that based on fundamental principles; we assume here that OH is not dissolved form in the molten metal phase.

The much higher stability of HBO gas in the system than other B-containing gas species (described in section II) indicate that B gasifies through the HBO formation. Since the equilibrium partial pressure of HBO gas is much higher than BH (Fig. 2), the formations of HBO through reactions (12) and (13) are the rete limited reactions, compared to HBO formation by reactions (14) to (16).

B.I Refining in quartz crucible

We observed that the rate of B removal is also depended upon the crucible material (Fig. 7). In a reactive system with significant amount of continuous gas supplying, the crucible material should not be the major factor to affect the gas phase composition and therefore the mass transport in the gas phase. However, the change of the crucible material affects the thermochemical properties of the melt and therefore for the B gasification in the system. When quartz crucible is used, the oxygen potential in the system and the activity of the

dissolved oxygen in the melt is higher compared to that in graphite crucible. Fig. 13 shows the calculated solubilities of oxygen in liquid silicon in quartz and graphite crucibles using the SINTEF solar grade silicon database.[18] Solubility of oxygen in liquid silicon in the quartz crucible is higher than that in graphite crucible under $p_{CO} = 0.0001$ atm (which is close to the equilibrium partial pressure of CO for silicon refining by H_2-3%H_2O), and during refining the real CO partial pressure is even lower. Oxygen solubility increases with increasing temperature in the quartz crucible, whereas it decreases with increasing temperature in graphite crucible, due mainly to the increase of carbon solubility. The relationship between the carbon saturation levels and the corresponding dissolved oxygen in different CO partial pressures are shown in Fig. 14. Regarding the oxygen solubility differences in quartz and graphite crucibles, it is therefore proposed that the faster B removal in quartz crucible can be attributed to the higher activity of the dissolved oxygen. Because the above reactions (14) and (15) do not involve the dissolved oxygen in the HBO gas formation, it is therefore concluded that HBO is formed mainly through chemical reaction (16). When graphite crucible is used, the required oxygen for HBO formation is obtained through chemical reactions (9) and (10). However, when quartz crucible is used an extra source of oxygen will be the following reaction on the crucible wall:

$$SiO_2(s) = Si + 2\,\underline{O} \qquad (17)$$

Reaction (17) is well-known to take place during, for example, single crystal pulling in the Cz process and is strongly affected by the fluid flow conditions in the crucible. During the refining, H_2O gas is continuously supplied into the system and SiO gas is produced continuously. Therefore, for both graphite and quartz crucibles, we assume that oxygen in the melt is always in or closed to saturation levels. The difference in the rates of HBO formation in these crucibles is due to the differences in the oxygen activity in the melt and rate of chemical reaction (16). This mechanism of B gasification, however, cannot be used to explain

the higher B removal rate in alumina crucible (Fig. 7), since the solubility of oxygen in silicon melts in equilibrium with alumina is lower than that with quartz crucible (Fig. 13).

B.II: Refining in alumina crucible

In order to explain the effect of alumina crucible on the B removal, the Si-Al-B-O-H system was studied using HSC Chemistry and FactSage thermodynamic software. It was found that when Al exists in the system, aluminum borate ($AlBO_2$) can be one of the important species in the gas phase, in addition to other Al-containing gas species such as Al_2O, AlH_3 and AlOH. Equilibrium calculations using the SINTEF solar grade silicon database[18] have then been carried out to estimate the influence of Al2O3 on the B removal. It was found that partial pressure of $AlBO_2$ is lower than that of HBO. The thermodynamic properties of $AlBO_2$ given by the JANAF thermochemical tables[20] seems not reliable, since it only used one unpublished report to evaluate the properties. The quantum chemistry calculations were carried out to determine the enthalpy and entropy of formation of $AlBO_2$ as described in the following.

Quantum chemistry techniques have reached a level of maturity such that the structures, spectroscopy and thermochemistry of small molecules can be calculated to an accuracy rivaling experiments.[21,22] We carried out calculations using the CCSD(T) (coupled cluster with single and double excitations and a perturbative treatment of triple excitations) method, since this is considered to be the "gold standard" of quantum chemistry, allowing to calculate energy differences to "chemical accuracy", i.e., with an error below 1 kcal/mol. In short, this involves calculating the correlation of electrons as an improvement on the mean-field Hartree-Fock electronic wave function that is used as a reference state. To calculate the heat of formation we ran calculations for both $AlBO_2$ and for the reference species B and Al atoms and O_2. We followed a procedure where first the molecular geometry was optimized using

CCSD(T) with the basis set aug-cc-pVQZ [23] for B and O and aug-cc-pV(Q+d)Z for Al [24] using the commonly employed frozen-core approximation. Subsequently, harmonic vibrational frequencies were calculated using the same method. Using the optimized geometries, frozen-core calculations with CCSD(T) and the larger aug-cc-pV6Z [25] and aug-cc-pV(6+d)Z [24] basis sets were carried out in order to approach the complete basis set limit. The calculated energy was further corrected for core-valence electron correlation, where not only valence but also outer core electrons (1s for B and O, 2s and 2p for Al) were correlated in the CCSD(T) calculations (using the cc-pwCV5Z basis set [26]). Finally, a first-order relativistic correction was added by employing all-electron CCSD(T) with an un-contracted cc-pVTZ [27,28] basis set and the DPT2 direct perturbation method [29,30]. All quantum chemistry calculations were performed using the CFOUR software package.[31]

The enthalpy of formation, standard entropy, and heat capacity were calculated by standard statistical thermodynamics equations [32] employing calculated vibrational frequencies, rigid-rotor rotational constants calculated from the optimized geometries and experimental data on electronic fine-structure states. [33] The standard states of B and Al at 298 K are the solid state, but for practical reasons B and Al atoms were used as reference species in the CCSD(T) calculations. We therefore employed the most accurate estimates of the heats of formation of B and Al atoms available, [34] to adjust the heat of formation to the correct reference value. Contrary to the assumptions made in JANAF, our calculations show that the $AlBO_2$ molecule is linear rather than bent (see Fig. XX), in agreement with recent experimental and theoretical results.[35] This affects the predicted thermodynamic properties. The JANAF heat of formation at 298 K was further estimated from experiments at 1500 K creating a relatively high uncertainty in the tabulated value. Indeed, there are clear, but not very large, differences between the calculated and JANAF values. The quantum chemistry results for $AlBO_2$ are an

enthalpy of formation of -524.2 kJ/mol (JANAF: -541.4 kJ/mol) and a standard entropy of 281.54 J/K mol (JANAF: 269.56 J/K mol). The calculated heat capacity is consistently higher than that in JANAF, 61.505 J/K mol (JANAF: 52.833 J/K mol) at room temperature and 85.164 J/K mol (JANAF: 80.972 J/K mol) at 2000 K. A conservative estimate of the accuracy of the heat of formation is obtained by summing up the expected uncertainties in the various contributions to total energy. The neglect of higher-order electron correlation in the CCSD(T) method should give at most 1 kcal/mol uncertainty, and not making an extrapolation to the complete basis set limit is expected to lead to an additional 0.5 kcal/mol uncertainty. [36] The error bars on the heats of formation of B and Al atoms are 0.2 kcal/mol and 0.4 kcal/mol, respectively. In summary, the maximum uncertainty of the heat of formation of $AlBO_2$ is therefore 2.1 kcal/mol or about 9 kJ/mol. It is highly likely that the actual inaccuracy is much less than this. The entropy and heat capacities are expected to be quite accurate.

Employing the above calculated enthalpy and entropy values in our solar grade silicon database,[18] the equilibrium partial pressures of HBO and $AlBO_2$ species in the gas phase were calculated for the refining of B in silicon melts in alumina crucible. The results are shown in Fig. 16. As we observe, the partial pressure of $AlBO_2$ gas is higher than HBO gas when silicon refining is carried out in alumina crucible. On the other hand, the thermodynamic calculations indicated that the partial pressures of HBO and $AlBO_2$ in the gas phase are dependent on the amount of Al_2O_3 for a given B concentration and temperature. Figure 17 shows the calculated relationships between the partial pressures of HBO and $AlBO_2$ and the amount of Al_2O_3. For the low values of Al_2O_3 in the system, the partial pressure of HBO is higher than $AlBO_2$ and vice versa. The equilibrium calculation results in Fig. 15 and 16 indicate that the total pressure of B-containing gas species is higher when alumina crucible is used. Boron may be removed through the formation of both HBO and $AlBO_2$.This can be used to explain the experimental observation: higher B removal rate in alumina crucible

compared to quartz and graphite crucibles. Three chemical reactions have thus been proposed here for the formation of $AlBO_2$ at the melt/crucible and the melt/gas interfaces as:

$$2/3Al_2O_3\,(s) + \underline{B} = AlBO_2(g) + 1/3\underline{Al} \qquad \Delta G°_{(1773\ K)} = 175.2\ kJ \qquad (18)$$

$$\underline{Al} + \underline{B} + 2H_2O(g) = AlBO_2(g) + 2H_2(g) \qquad \Delta G°_{(1773\ K)} = -265.6\ kJ \qquad (19)$$

$$\underline{Al} + \underline{B} + 2\underline{O} = AlBO_2(g) \qquad \Delta G°_{(1773\ K)} = -670.7\ kJ \qquad (20)$$

The dissolved Al for chemical reactions (19) and (20) is provided through the following reaction on the crucible wall:

$$Al_2O_3\,(s) = 2\underline{Al} + 3\,\underline{O} \qquad (21)$$

Based on the experimental observations, the concentration of Al in the melt reaches to levels around 2000 ppmw, which is close to the equilibrium concentration determined by equilibrium simulations. Hence, there is always high concentration of Al in the melt for the chemical reactions (19) and (20). Although the $\Delta G°$ value for the chemical reaction (18) shows a positive number, the reaction can occur due to the low chemical activity of Al[37] and low partial pressure of $AlBO_2$. However, from thermodynamic point of view the $AlBO_2$ formation through the chemical reactions (19) and (20) is more favorable. Since they provide higher equilibrium partial pressures compared to chemical reaction (18). Bothe reactions (19) and (20) give close partial pressures of $AlBO_2$ to those in Fig. 17. The equilibrium partial pressures of $AlBO_2$ obtained for reaction (18) are in the range of 1×10^{-9} to 1×10^{-11} atm. Considering similar equilibrium partial pressures for $AlBO_2$ for chemical reactions (19) and (20), we have the same driving forces for the reactions. From kinetics point of view, however, the adsorbed H_2O on the melt surface reacts mainly with Si and Al to form SiO, AlH_3 and AlOH gases, and therefore the B gasification through chemical reaction (20) may be more favorable. The equilibrium partial pressures of AlH_3 and AlOH gases in the system are higher

than $AlBO_2$ and if Al at the surface gets contact with H_2O, formation of these gases is more favorable than the formation of $AlBO_2$ through chemical reaction (19). Aluminum and oxygen are continuously transferred into the melt through chemical reaction (21). These elements are available all over the melt and for chemical reaction (20) in a large interfacial area; both melt/crucible and melt/gas interfaces.

C. Effect of temperature on B removal

In order to discuss the effect of temperature on the B removal kinetics, we consider here the possible chemical reactions for the formation of SiO gas:

$$Si + [H_2O]^{ads.} = SiO\ (g) + 2\ \underline{H}\ \ (\text{or } [H]^{ads.} \text{ or } H_2) \quad (22)$$

$$Si + [OH]^{ads.} = SiO\ (g) + \underline{H}\ \ \ (\text{or } [H]^{ads.}) \quad (23)$$

$$Si + \underline{O}\ (\text{or } [O]^{ads.}) = SiO\ (g) \quad (24)$$

The formation of SiO gas through reactions (22) and (23) has no effect on the B removal kinetics, since HBO gas is mainly formed through reaction (16) in graphite and quartz crucibles. Although the SiO gas formation through reaction (22), with or without the contribution of reaction (6), can be the most important reaction for SiO gas formation, the most significant reaction which affects HBO formation is the chemical reaction (24) due to the role of the dissolved oxygen. Fig. 18 shows the calculated partial pressures for HBO and SiO gaseous species for a given B concentration at 30 ppmw at different temperatures. The magnitude of *pSiO/pHBO* ratio indicate that the formation of SiO gas at the surface is more favorable compared to HBO gas. Hence, Si reacts rapidly with $\underline{O}$ (or $O^{ads.}$) on the surface and it prevents the adjacent B atoms to react with these species. According to Fig. 18, p_{SiO}/p_{HBO} ratio increases with increasing temperature. This means higher relative activity of activated

complex of SiO than the activated complex of HBO at the melt surface. The effect of temperature on the B removal kinetics was previously proposed to be due to the lower HBO partial pressure at higher temperatures. However, it is more precise to say it is due to the increase in *pSiO/pHBO* ratio as illustrated in Fig.16. In other words, the oxygen atom at the melt surface oxidizes Si to SiO gas and is less reactive to oxidize the adjacent B to HBO gas. Since the rate of SiO gas formation at lower temperatures is slower for given H_2O supply to the system, the adsorbed H_2O on the melt surface will have a higher chance to provide O atoms by reactions (9) and (10), which means higher possibility of HBO formation by reaction (16) at lower temperatures. Therefore, we may propose that the rate of B removal is also controlled by the rate of dissolved oxygen supply to the system, in addition to the mass transport in the gas phase.

D. Summary of the mechanism of B removal

Based on the above discussions, the mechanism of B removal from silicon by H_2-H_2O gas mixtures can be proposed as schematically shown in Fig. 19, depending on the crucible material. When refining is carried out in graphite and quartz crucibles, H_2 and H_2O dissociations at the melt surface provide adsorbed or dissolved H and O atoms. These elements can further gasify B to HBO and Si to SiO. Oxygen transfer to the melt from quartz crucible can provide a limited amount of oxygen compared to the H_2O gas. When an alumina crucible is used, Al and O atoms are rapidly transferred to the melt and boron is gasified also to $AlBO_2$ at the melt surface and even on the crucible wall. The competitiveness of the HBO and $AlBO_2$ formation, when alumina crucible is used, is depending on the equilibrium partial pressures of this species. The formation of SiO gas through direct reaction with H_2O is the main reaction for SiO formation, since the oxygen solubility is limited to low concentrations.

VI. Conclusions

The removal of B from B-doped silicon melts was studied through the application of top gas blowing of humidified hydrogen. The effect of process parameters; temperature, lance diameter, lance distance from the melt, gas flow rate, and crucible material on the kinetics of B removal was studied and rate constants were determined. It was observed that the rate of B removal is decreased with increasing temperature, which is attributed to the competitiveness of Si and B to oxidation, which can be indicated by the increases of the equilibrium p_{SiO}/p_{HBO} ratio in the system, when refining is performed in graphite and quartz crucibles. It was also observed that the rate of B removal is increased with increasing the flow rate of the gas and a linear relationship between the two parameters was determined. CFD modeling of the refining system indicates that in higher gas flow rates we obtain more extend of the refining gas over the melt surface which increases the mass transport of both gaseous reactants and products in the gas phase. It was found that the rate of B removal in alumina crucible is the highest followed by that in quartz and graphite crucibles. Faster B removal in quartz crucible than graphite crucible is proposed to be attributed to the oxygen potential in the system and the role of the dissolved oxygen in silicon. On the other hand, the faster B removal in alumina crucible is attributed to B gasification through $AlBO_2$ formation in addition to HBO formation. It is proposed that the B removal from silicon by humidified hydrogen is a mix-controlled process by both chemical reaction and mass transport in the gas phase. It was proposed that the B gasification from the silicon melt occurs through its interaction with the dissolved elements:

In graphite, quartz and alumina crucible: $\underline{B} + \underline{H} + \underline{O} = HBO\ (g)$

In alumina crucible: $\underline{Al} + \underline{B} + \underline{O} = AlBO_2\ (g)$

According to the present study, the quantum chemistry results for $AlBO_2$ are an enthalpy of formation of -524.2 kJ/mol and standard entropy of formation 281.54 J/K mol.

Table Captions:

Table I: The details of the experiments in the present study.

Exp. No.	Crucible Type	Temperature K (°C)	Lance Diameter (mm)	Lance distance to melt surface (mm)	Gas flow rate (NL/min)	Mass trasfer coefficient (m/s)
1	Graphite	1703 (1430)	4	30	0.5	2.0×10^{-6}
2	Graphite	1703 (1430)	4	30	1.5	3.3×10^{-6}
3	Graphite	1703 (1430)	4	30	3	1.3×10^{-5}
4	Graphite	1703 (1430)	2	30	0.5	1.5×10^{-6}
5	Graphite	1703 (1430)	2	30	1.5	5.1×10^{-6}
6	Graphite	1703 (1430)	2	30	3	9.4×10^{-6}
7	Graphite	1703 (1430)	2	30	6	1.9×10^{-5}
8	Graphite	1703 (1430)	2	30	9	2.5×10^{-5}
9	Graphite	1703 (1430)	2	10	6	1.3×10^{-5}
10	Graphite	1703 (1430)	2	50	6	1.7×10^{-5}
11	Graphite	1803 (1530)	4	30	3	7.0×10^{-6}
12	Graphite	1803 (1530)	2	30	6	1.3×10^{-5}
13	Alumina	1773 (1500)	2	30	3	2.1×10^{-5}
14	Quartz	1703 (1430)	2	30	3	1.5×10^{-5}
15	Quartz	1773 (1500)	2	30	3	1.4×10^{-5}

Figure captions:

Figure 1: Sketch of the Si-B-H-O system and the stable compounds in its binary systems.

Figure 2: Equilibrium partial pressures of the gas species above 400 g Si-B melts in contact with H_2-3vol%H_2O gas at 1430°C.

Figure 3: Schematic of the experimental set up for silicon refining by top gas blowing technique.

Figure 4: Boron concentration changes in silicon under different gas flow rates for given experimental conditions.

Figure 5: Boron concentration changes in silicon in different lance tip distances from the melt surface and given experimental conditions.

Figure 6: Boron concentration changes in silicon in different temperatures and given experimental conditions.

Figure 7: Boron removal from silicon in different crucibles and given experimental conditions.

Figure 8: Relationship between $ln\ (C_{B,i}/C_{B,t})$ and $(A/V)t$ for different gas flow rates and fixed other refining conditions in graphite crucible.

Figure 9: Correlation between the determined total mass transfer coefficients and the applied gas flow rates.

Figure 10: Velocity magnitude illustrating the effect of flow rate, lance distance, and lance diameter.

Figure 11: Average radial velocity above the metal surface for different gas flow rates and considering a 2mm lance positioned 3 cm above the surface.

Figure 12: Average radial velocity above the metal surface for different lance positions above the surface for 2 mm lance and 6 NL/min gas flow rate.

Figure 13: Calculated solubility of oxygen in liquid silicon in quartz, alumina and graphite crucibles for different temperatures. Calculated carbon solubility in silicon in graphite crucible is also given.

Figure 14: Calculated relationship between the solubility of oxygen and carbon concentration in liquid silicon.

Figure 15: Molecular structure of $AlBO_2$ with calculated bond lengths in Å.

Figure 16: The equilibrium partial pressures of HBO and $AlBO_2$ above the dilute solutions of B in liquid silicon in different crucibles at 1500°C in contact with one mole H_2-3%H_2O gas.

Figure 17: The equilibrium partial pressures of HBO and $AlBO_2$ above liquid silicon containing 30 ppmw B at 1500°C in contact with different amounts of alumina and one mole H_2-3%H_2O gas mixture.

Figure 18: The relationship between the p_{HBO} and p_{SiO} and p_{SiO}/p_{HBO} ratio and temperature for Si melt containing 30 ppmw boron.

Figure 19: Schematic of the mechanism of B removal and Si loss and the main related reactions in different refining systems.

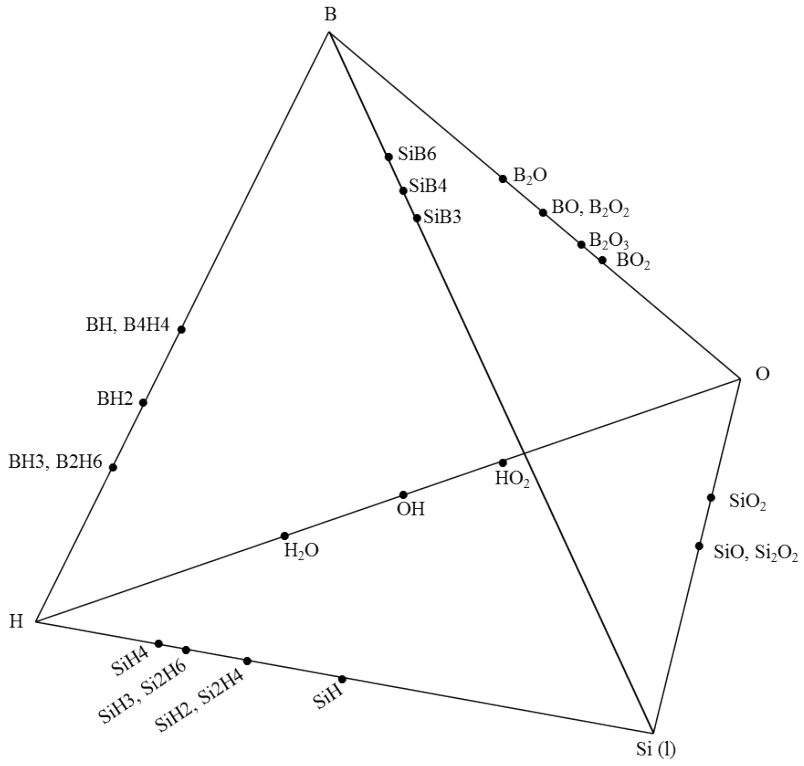

Figure 1: Sketch of the Si-B-H-O system and the stable compounds in its binary systems.

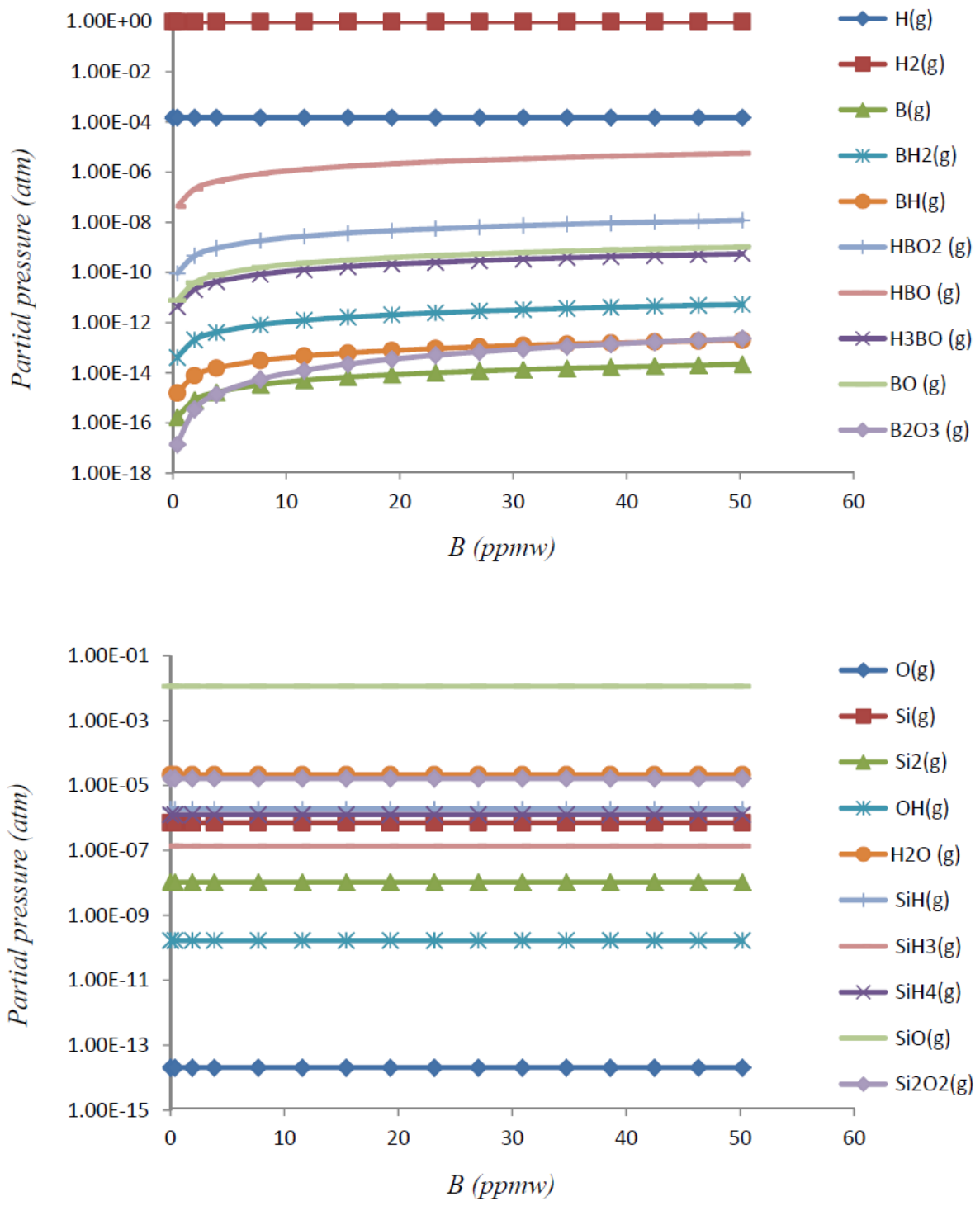

Figure 2: Equilibrium partial pressures of the gas species above 400 g Si-B melts in contact with H_2-3vol%H_2O gas at 1430°C.

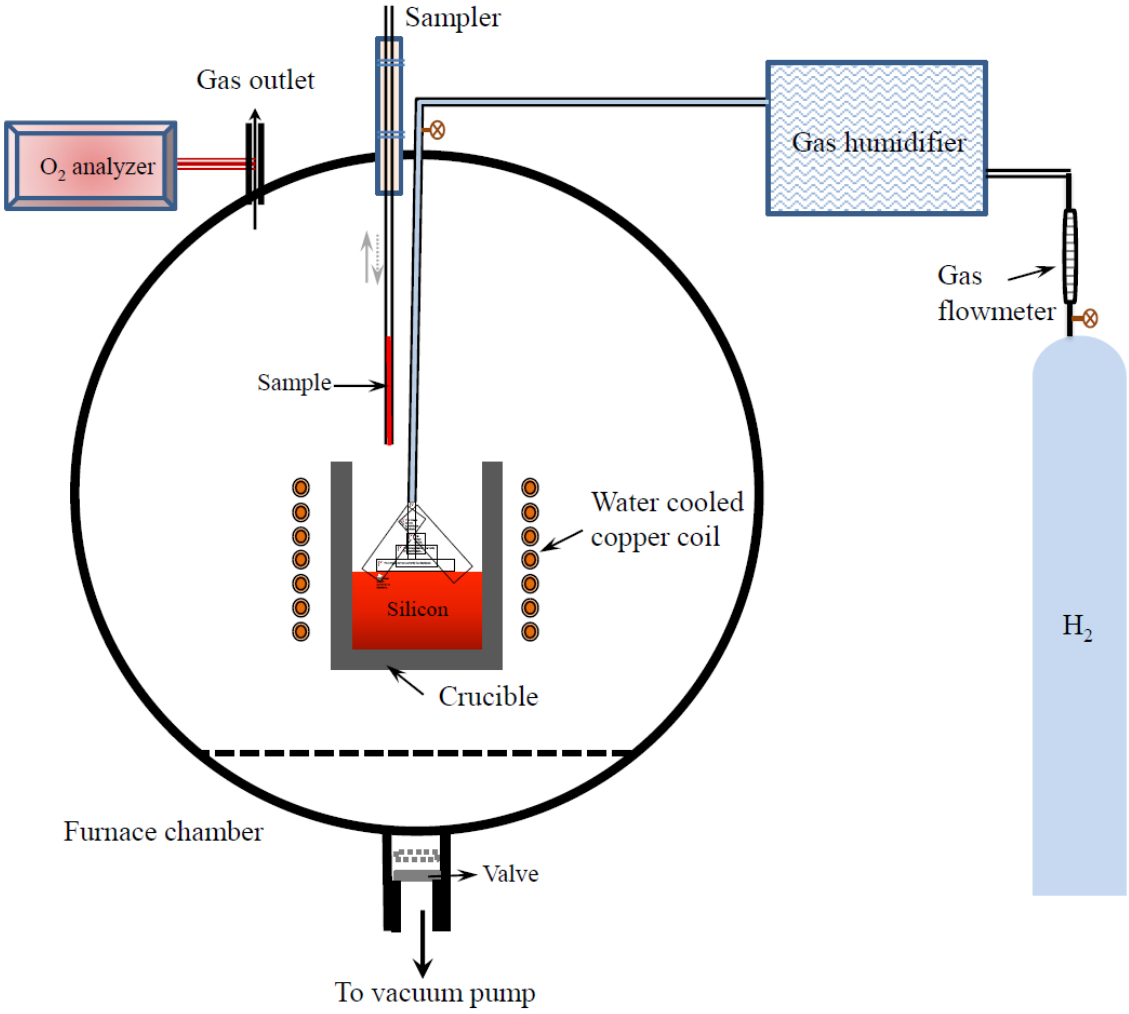

Figure 3: Schematic of the experimental set up for silicon refining by top gas blowing technique.

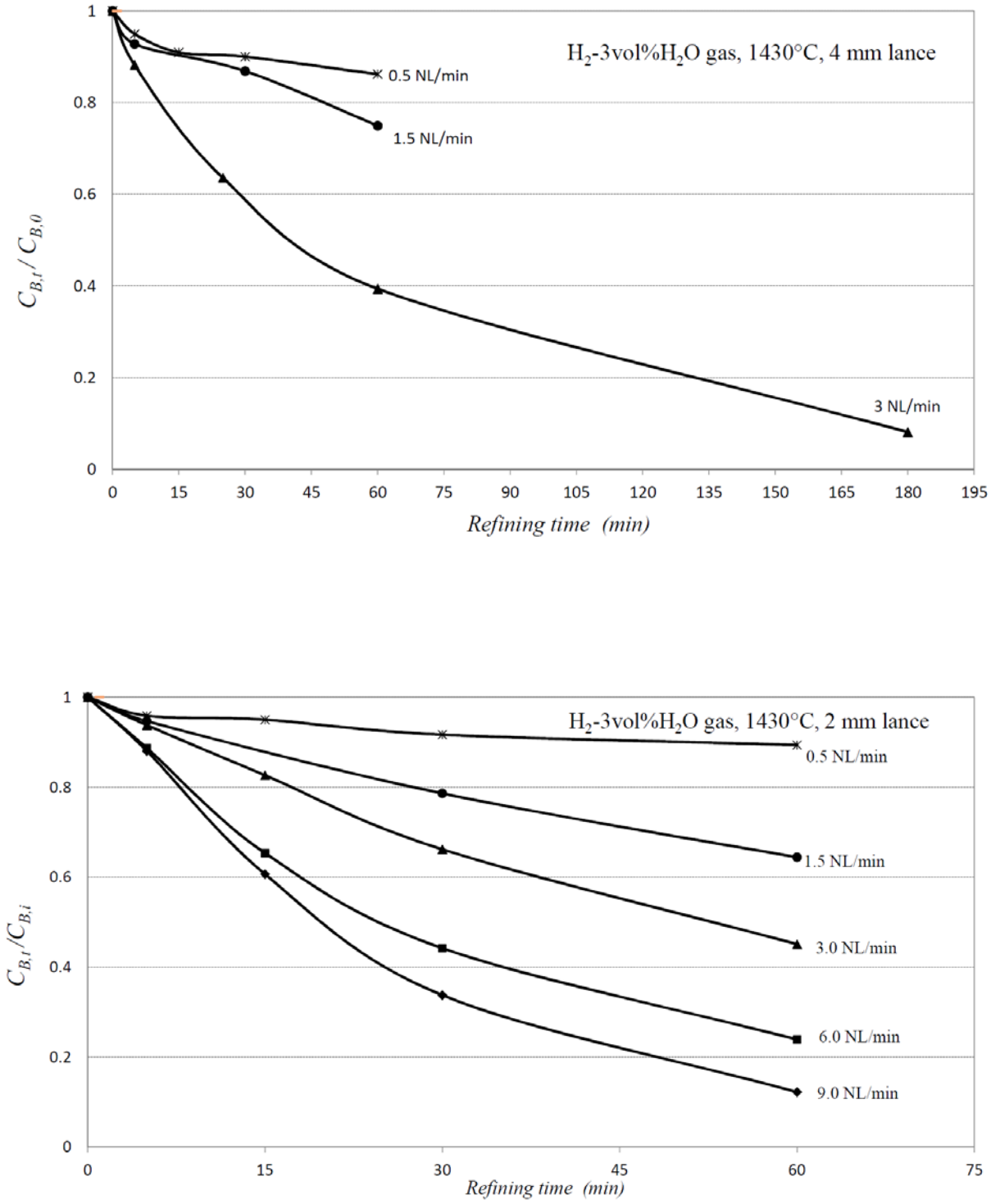

Figure 4: Boron concentration changes in silicon under different gas flow rates for given experimental conditions.

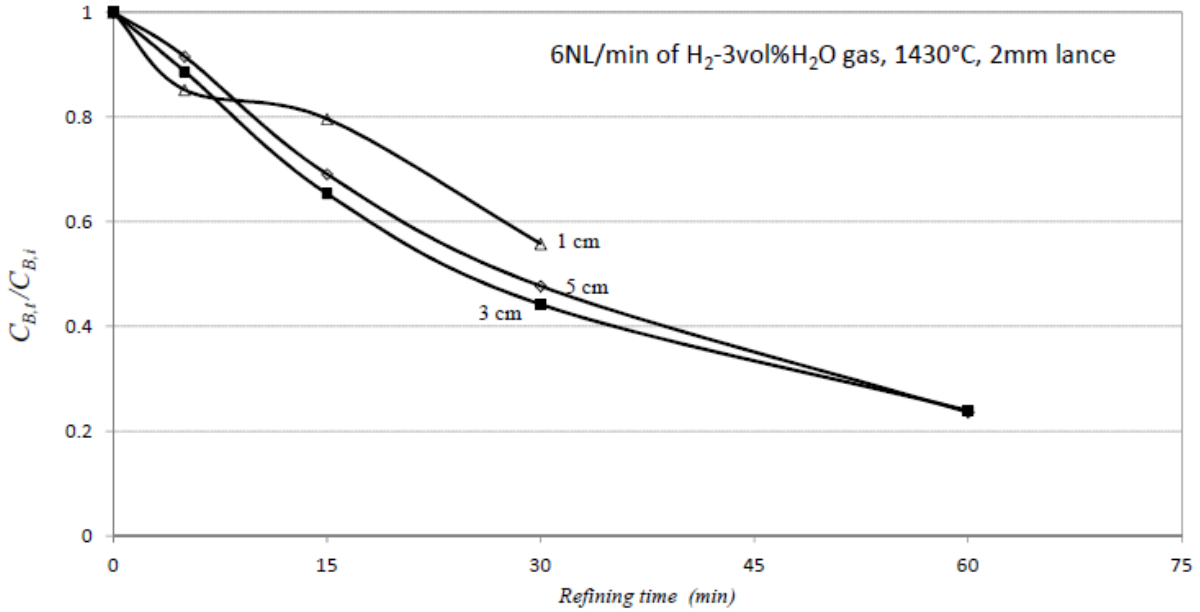

Figure 5: Boron concentration changes in silicon in different lance tip distances from the melt surface and given experimental conditions.

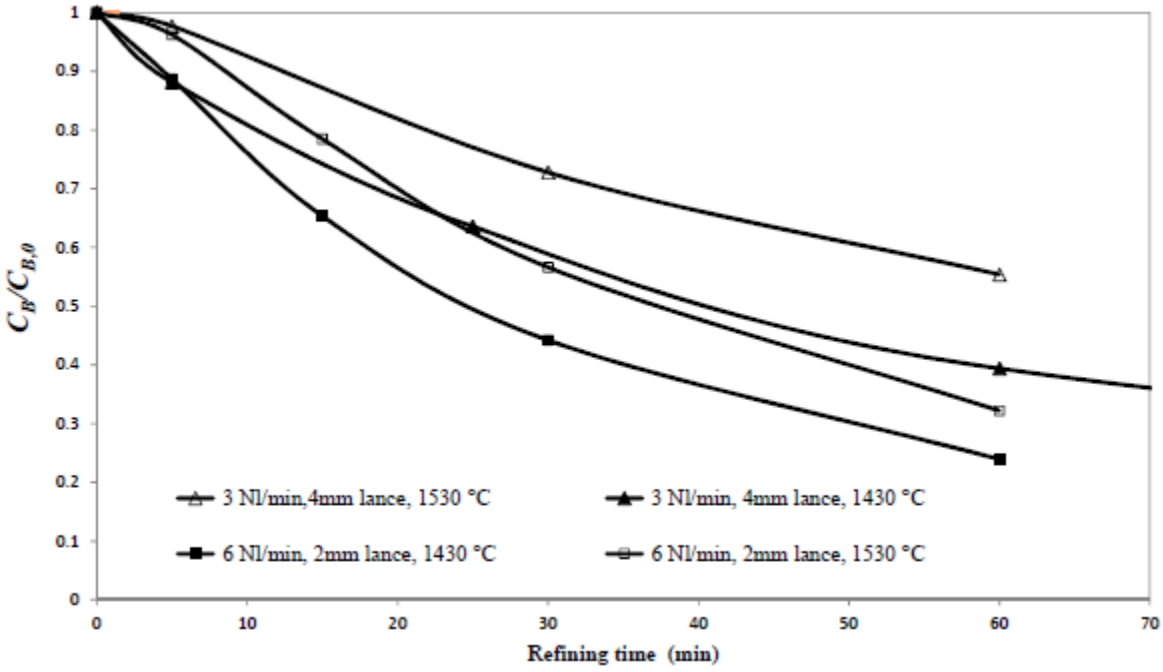

Figure 6: Boron concentration changes in silicon in different temperatures and given experimental conditions.

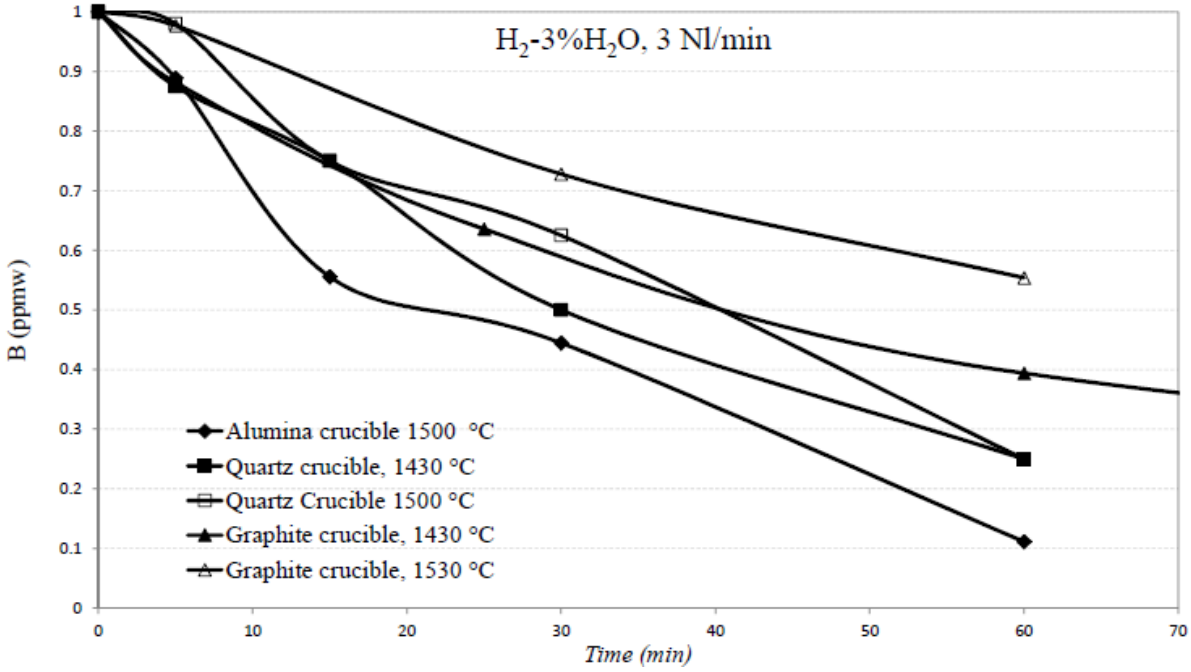

Figure 7: Boron removal from silicon in different crucibles and given experimental conditions.

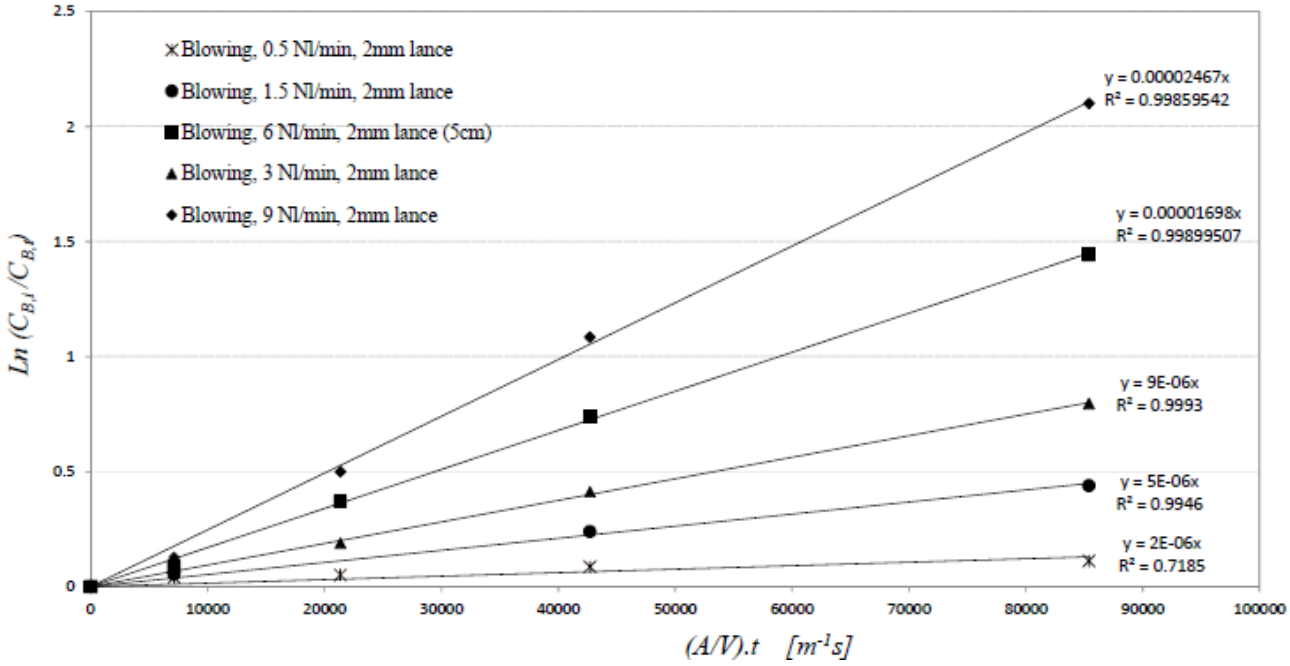

Figure 8: Relationship between *ln* $(C_{B,i}/C_{B,t})$ and *(A/V)t* for different gas flow rates and fixed other refining conditions in graphite crucible.

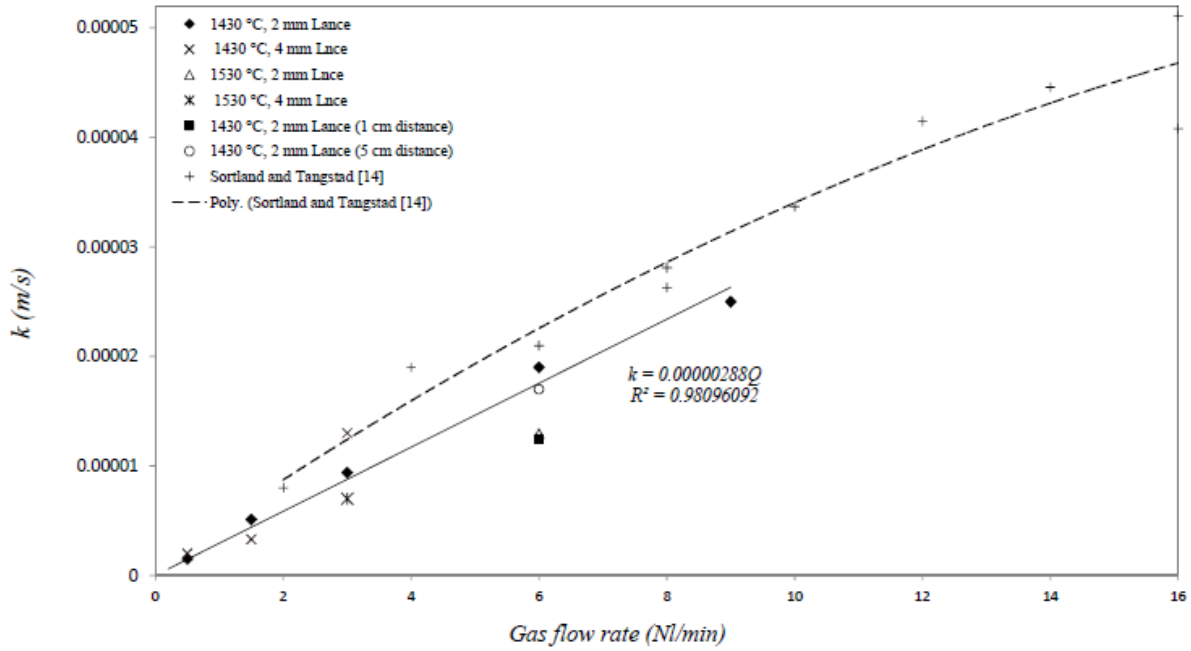

Figure 9: Correlation between the determined total mass transfer coefficients and the applied gas flow rates.

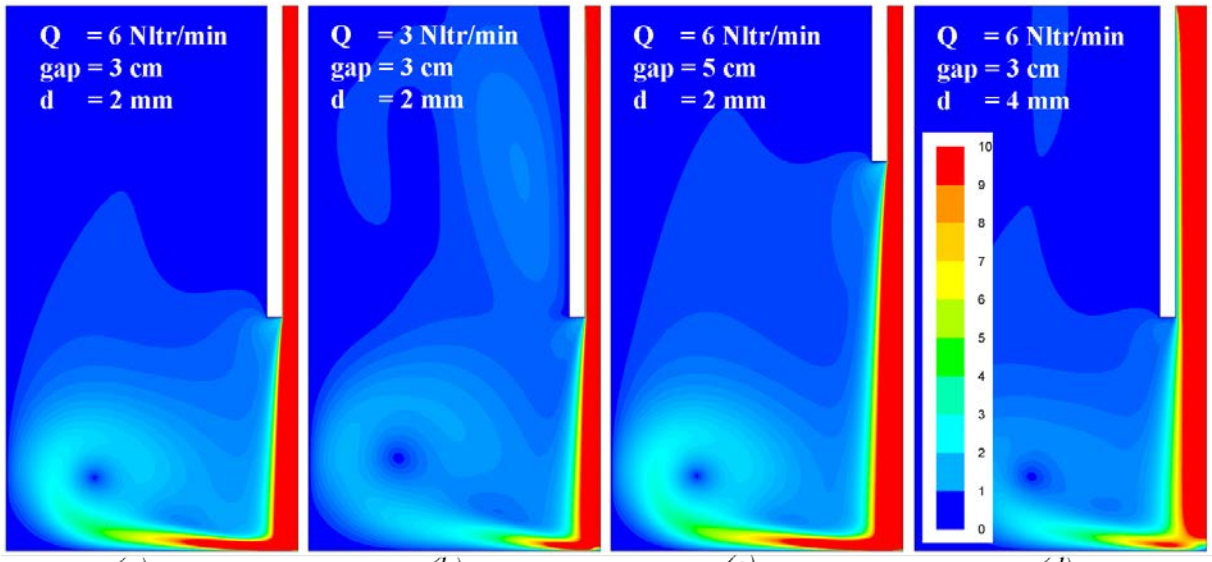

Figure 10: Velocity magnitude illustrating the effect of flow rate, lance distance, and lance diameter.

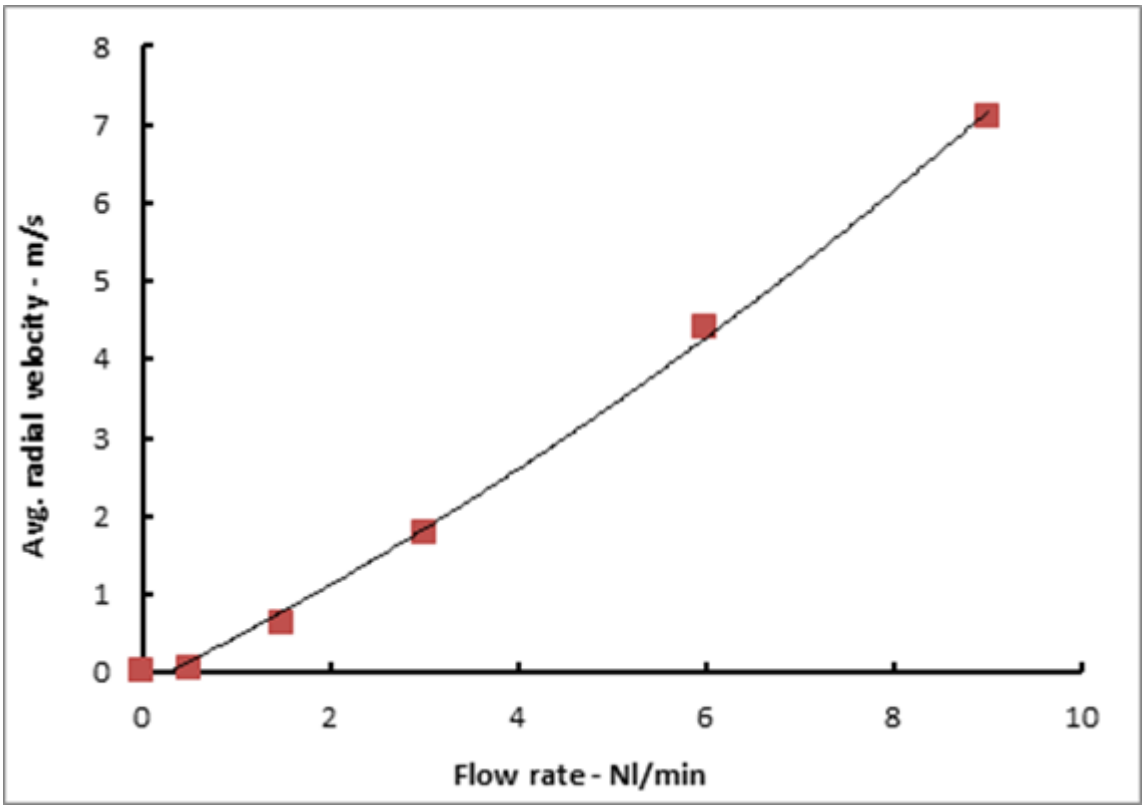

Figure 11: Average radial velocity above the metal surface for different gas flow rates and considering a 2mm lance positioned 3 cm above the surface.

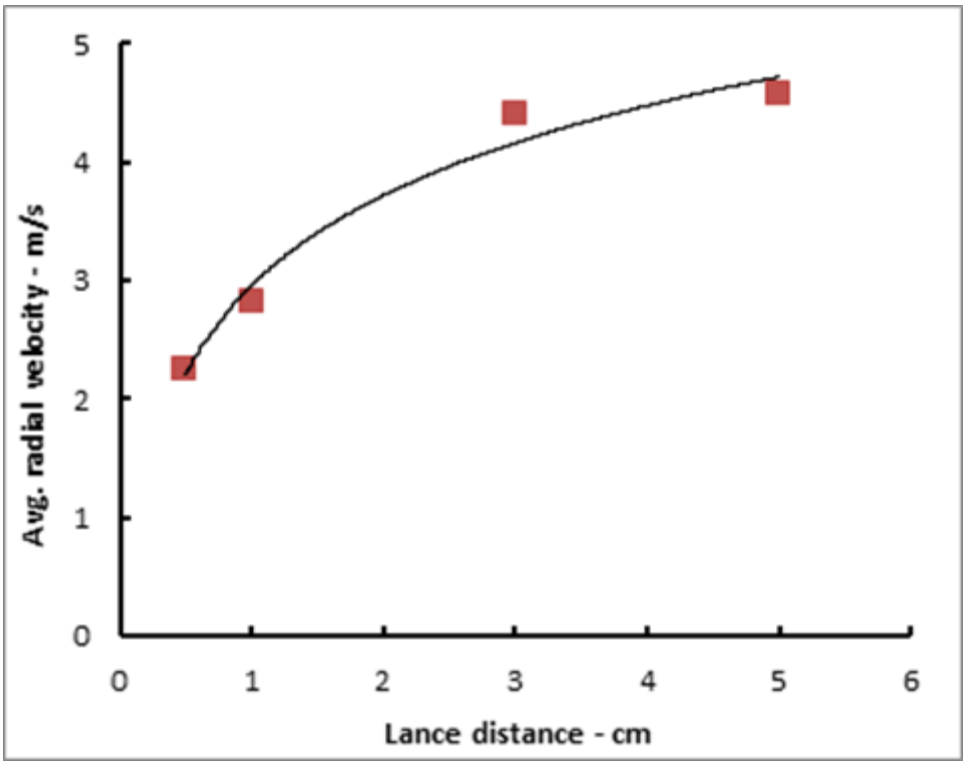

Figure 12: Average radial velocity above the metal surface for different lance positions above the surface for 2 mm lance and 6 NL/min gas flow rate.

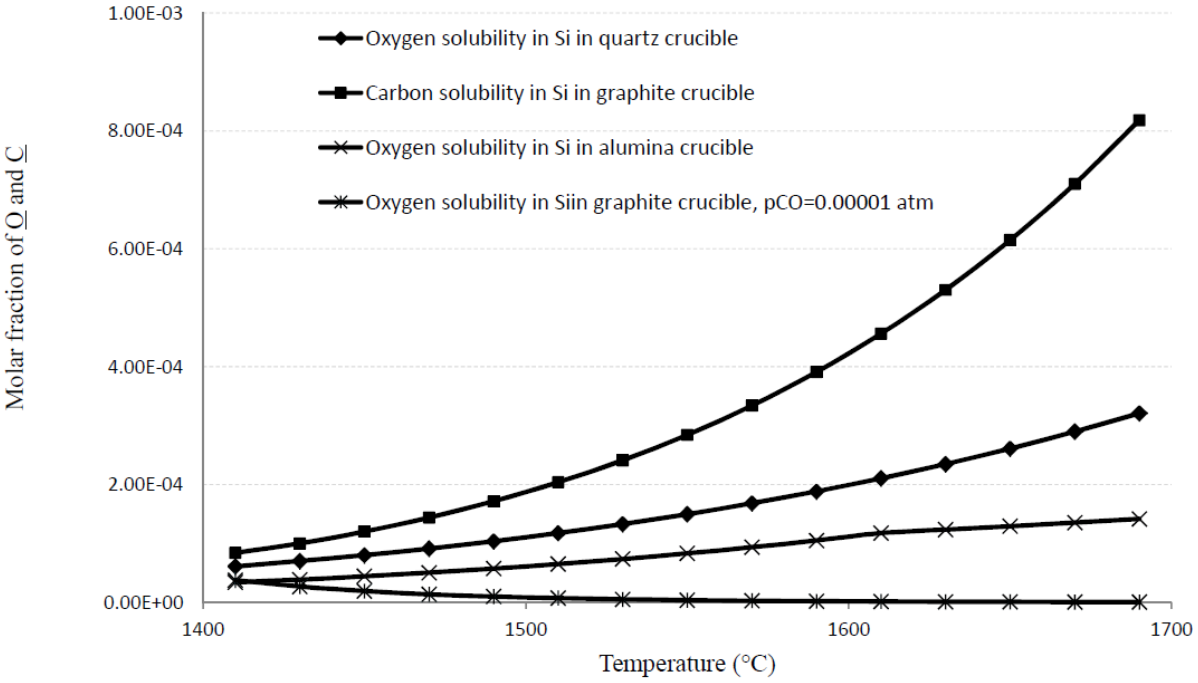

Fig. 13: Calculated solubility of oxygen in liquid silicon in quartz, alumina and graphite crucibles for different temperatures. Calculated carbon solubility in silicon in graphite crucible is also given.

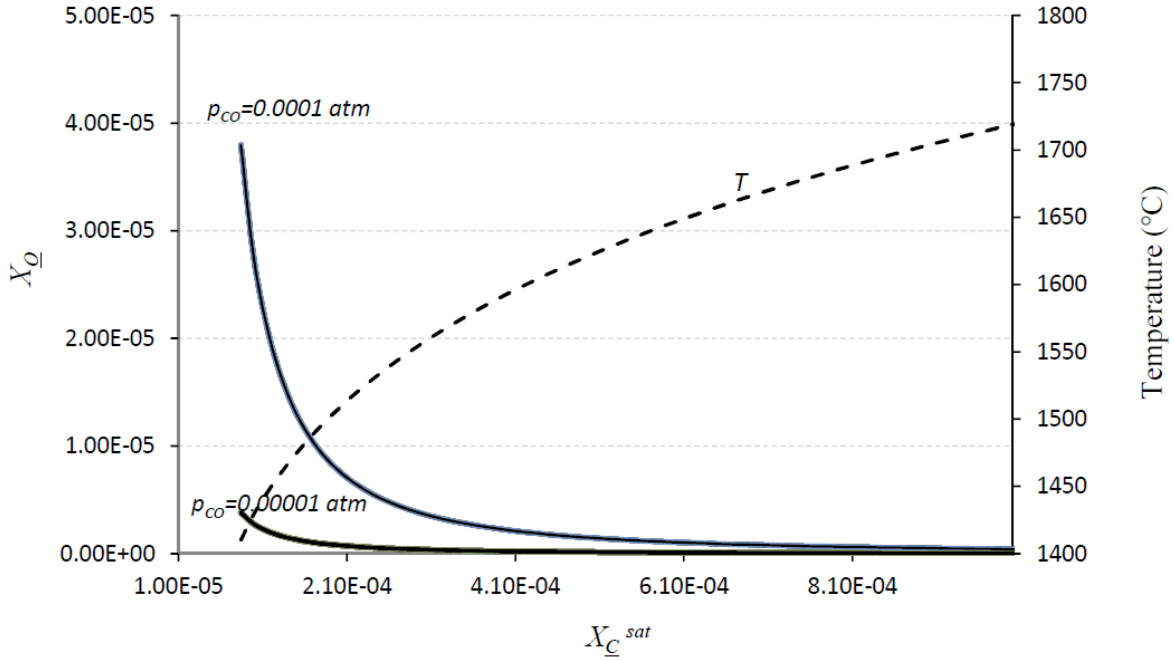

Figure 14: Calculated relationship between the solubility of oxygen and carbon concentration in liquid silicon.

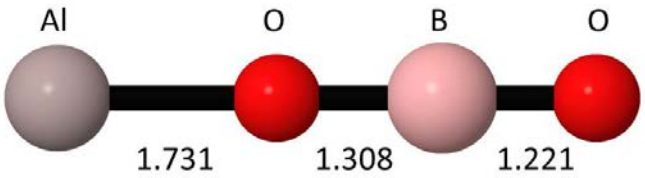

Figure 15: Molecular structure of $AlBO_2$ with calculated bond lengths in Å.

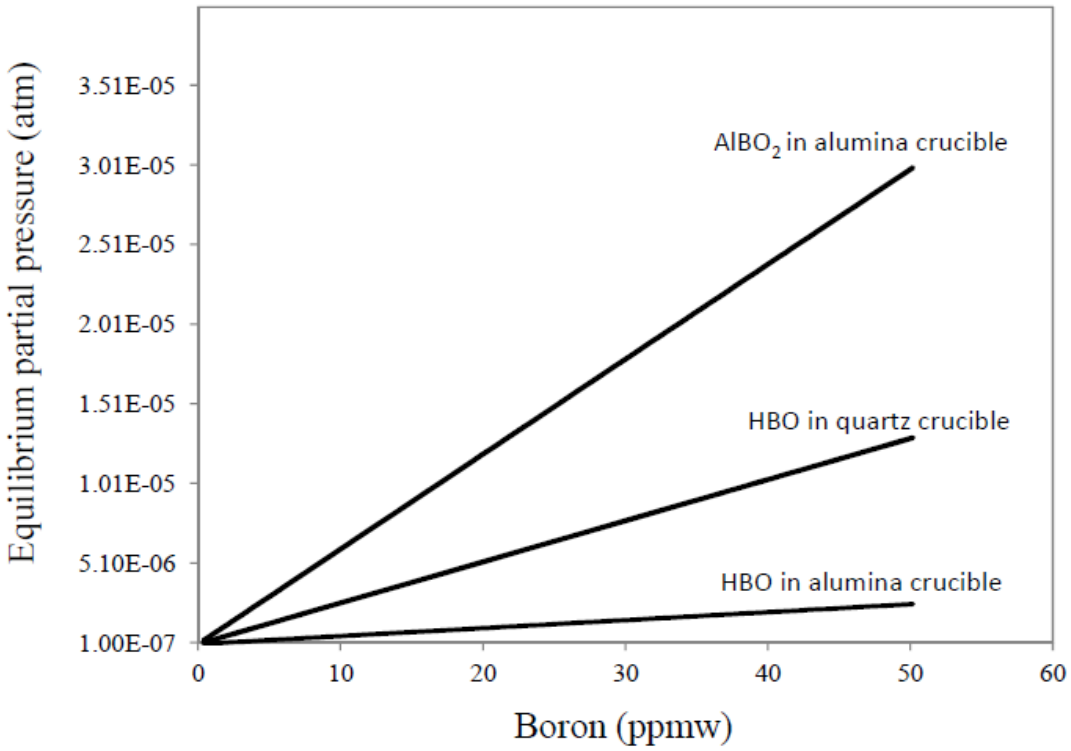

Figure 16: The equilibrium partial pressures of HBO and $AlBO_2$ above the dilute solutions of B in liquid silicon in different crucibles at 1500°C in contact with one mole H_2-3%H_2O gas.

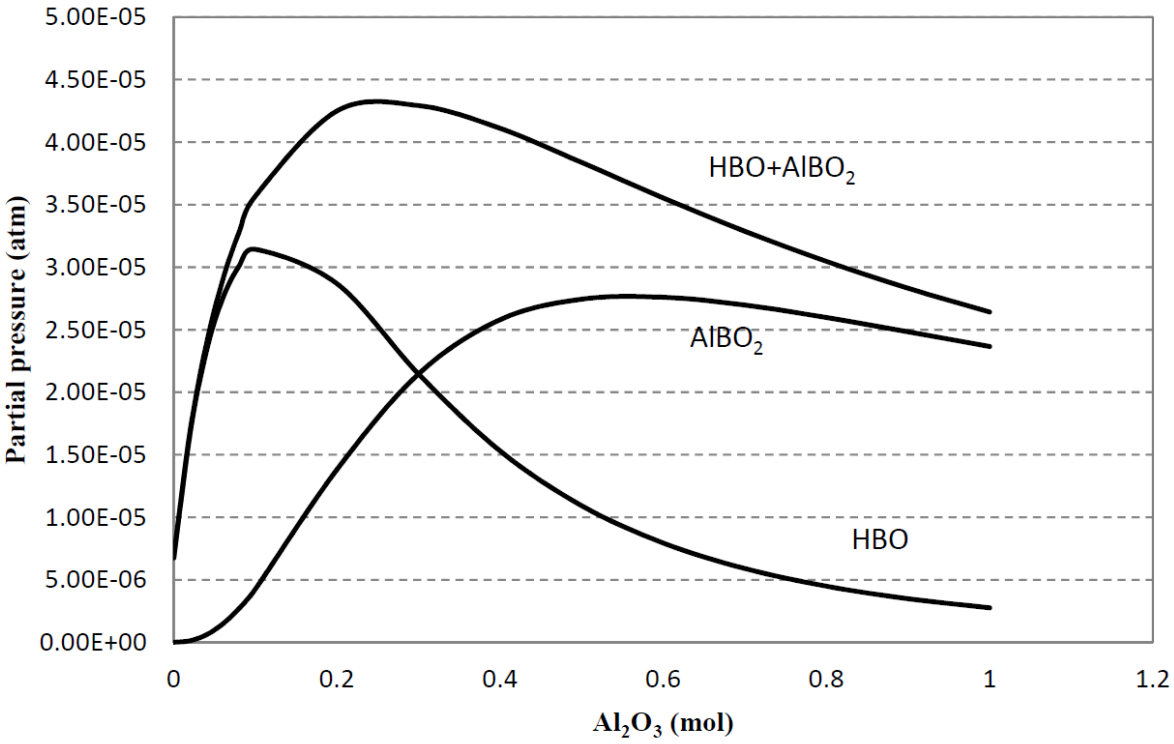

Figure 17: The equilibrium partial pressures of HBO and $AlBO_2$ above liquid silicon containing 30 ppmw B at 1500°C in contact with different amounts of alumina and one mole H_2-3%H_2O gas mixture.

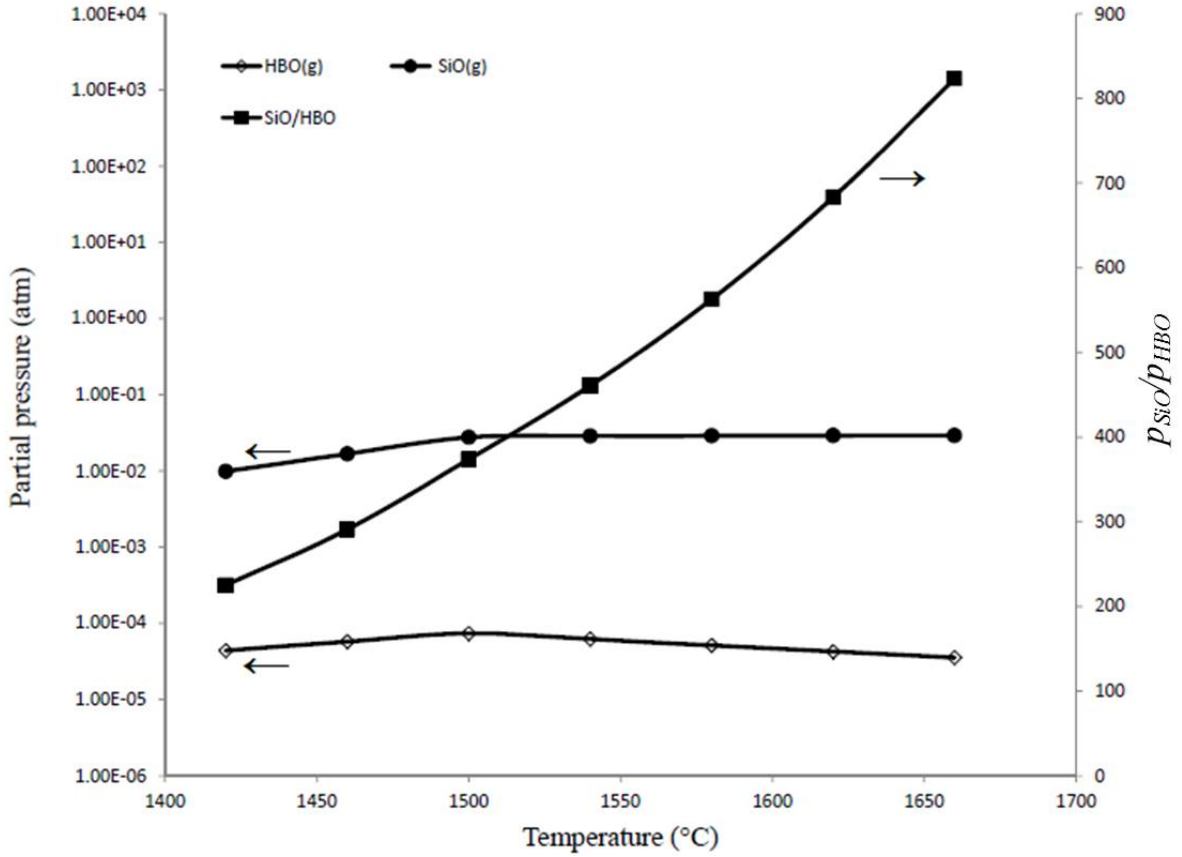

Figure 18: The relationship between the p_{HBO} and p_{SiO} and p_{SiO}/p_{HBO} ratio and temperature for Si melt containing 30 ppmw boron.

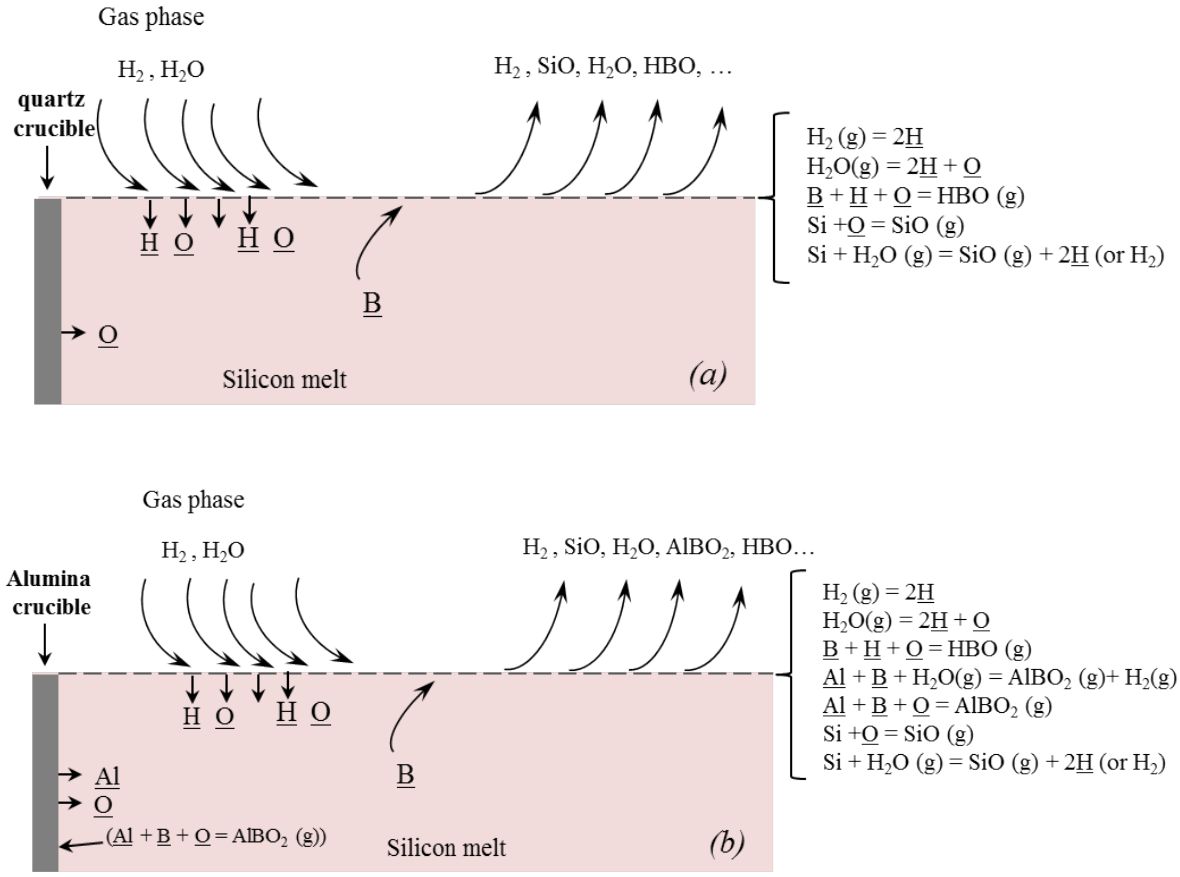

Figure 19: Schematic of the mechanism of B removal and Si loss and the main related reactions in different refining systems.

References

[1] J. Safarian, G. Tranell, M. Tangstad: Energy Procedia, Vol. 20 (2012), pp. 88 – 97.

[2] S. Tsao and S.S. Lian: Mater. Sci. Forum, 2005, vols. 475–479,pp. 2595–98

[3] K. Suzuki, K. Sakaguchi, T. Nakagiri, and N. Sano: J. Jpn. Inst. Met., 1990, vol. 54, pp. 161–67.

[4] E. Nordstrand and M. Tangstad: Metall. Mat.. Trans. B, 2012, vol. 43B, pp. 814–22.

[5] S. Rousseau, M. Benmansour, D. Morvan, and J. Amouroux: Sol. Energy Mater. Sol. Cells, 2007, vol. 91, pp. 1906–15.

[6] T. Ikeda and M. Maeda: Mater. Trans., 1996, vol. 37, pp. 983–87.

[7] Khattak C.P., Joyce D.B., and Schmid F.: Report NREL/SR-520-27593, National Renewable Energy Laboratory, 1999.

[8] C.P. Khattak, D.B. Joyce, and F. Schmid: Sol. Energy Mater. Sol. Cells, 2002, vol. 74, pp. 77–89.

[9] N. Yuge, M. Abe, K. Hanazawa, H. Baba, N. Nakamura, Y. Kato, Y. Sakaguchi, S. Hiwasa, and F. Aratani: Prog. Photovolt.Res. Appl., 2001, vol. 9, pp. 203–209.

[10] N. Nakamura, H. Baba, Y. Sakaguchi, and Y. Kato: Mater. Trans., 2004, vol. 45 (3), pp. 858–64.

[11] J.J. Wu, W.H. Ma, Y.N. Dai, and K. Morita: Trans. Nonferr. Met. Soc. China, 2009, vol. 19, pp. 463–67.

[12] J. Safarian, K. Tang, K. Hildal, G. Tranell: Metall. Mater. Trans. E, 2014, vol. 1E, pp. 41-47.

[13] C. Alemany, C. Trassy, B. Pateyron, K.-I. Li, and Y. Delannoy: Sol. Energy Mater. Sol. Cells, 2002, vol. 72, pp. 41–48.

[14] E. Fourmond, C. Ndzogha, D. Pelletier, Y. Delannoy, C. Trassy, Y. Caratini, Y. Baluais, and R. Einhaus: 19th European Photovoltaic Solar Energy Conference, Paris, France, 7–11 June, 2004.

[15] Ø.S. Sortland, M. Tangstad: Metall. Mater. Trans. E, 2014, vol. 1E, pp. 211-25.

[16] K. Tang, S. Andersson, E. Nordstrand, and M. Tangstad: JOM, 2012, vol. 64 (8), pp. 952–56.

[17] V. D. Eisenhüttenleute: Slag Atlas, 2nd ed., Verlag Stahleisen GmbH, Dusseldorf, Germany, 1995.

[18] K. Tang, E.J. Øvrelid, G. Tranell, and M. Tangstad: 12th International Ferroalloys Congress, June 6–9, Helsinki, Finland, 2010, pp. 619–29.

[19] M. Næss, G. Tranell, J.E. Olsen, N. Kamfjord, K. Tang: Oxidation of Metals, Vol. 78 (2012), pp. 239-251.

[20] M.W. Chase, NIST-JANAF Thermochemical Tables, 4th Ed., NIST, 1998.

[21] D. Feller, K.A. Peterson, and D.A. Dixon: J. Chem. Phys., 2008, vol. 129 (20), 204105

[22] K.A. Peterson, D. Feller, and D.A. Dixon: Theor. Chem. Acc., 2012, vol. 131 (1), 1079.

[23] R.A. Kendall, T.H. Dunning, Jr., and R.J. Harrison: J. Chem. Phys., 1992, vol. 96 (9), pp. 6796-6806.

[24] T.H. Dunning, Jr., K.A. Peterson, and A.K. Wilson: J. Chem. Phys., 2001, vol. 114 (21), pp. 9244-9253.

[25] T. Van Mourik, A.K. Wilson, and T.H. Dunning, Jr.: Mol. Phys., 1999, vol. 96 (4), pp. 529-547.

[26] K.A. Peterson and T.H. Dunning, Jr.: J. Chem. Phys., 2002, vol. 117 (23), pp. 10548-10560.

[27] T.H. Dunning, Jr.: J. Chem. Phys., 1989, vol. 90 (2), pp. 1007-1023.

[28] D.E. Woon and T.H. Dunning, Jr.: J. Chem. Phys., 1993, vol. 98 (2), pp. 1358-1371.

[29] W. Klopper, J. Comp. Chem., 1997, vol. 18 (1), pp. 20-27.

[30] S. Stopkowicz and J. Gauss: J. Chem. Phys., vol. 129 (16), 164119.

[31] CFOUR, Coupled-Cluster techniques for Computational Chemistry, a quantum-chemical program package by J.F. Stanton, J. Gauss, M.E. Harding, P.G. Szalay
with contributions from A.A. Auer, R.J. Bartlett, U. Benedikt, C. Berger, D.E. Bernholdt, Y.J. Bomble, L. Cheng, O. Christiansen, M. Heckert, O. Heun, C. Huber, T.-C. Jagau, D. Jonsson, J. Jusélius, K. Klein, W.J. Lauderdale, D.A. Matthews, T. Metzroth, L.A. Mück, D.P. O'Neill, D.R. Price, E. Prochnow, C. Puzzarini, K. Ruud, F. Schiffmann, W. Schwalbach, C. Simmons, S. Stopkowicz, A. Tajti, J. Vázquez, F. Wang, J.D. Watts and the integral packages MOLECULE (J. Almlöf and P.R. Taylor), PROPS (P.R. Taylor), ABACUS (T. Helgaker, H.J. Aa. Jensen, P. Jørgensen, and J. Olsen), and ECP routines by A. V. Mitin and C. van Wüllen. For the current version, see http://www.cfour.de.

[32] C. E. Hecht: Statistical Thermodynamics and Kinetic Theory, W. H. Freeman, New York, 1990

[33] C. E. Moore: “Atomic energy levels”, Natl. Bur. Stand. Ref. Data Ser., Natl. Bur. of Stand. (U.S), Circ. No. 35 (U.S. GPO, Washington D.C., 1971.

[34] A. Karton and J. M. L. Martin: J. Phys. Chem. A., 2007, vol. 111 (26), pp. 5936-5944.

[35] G. Wang, M. Chen., G. Jiang, H. Zhou, and M. Zhou: Chem. Phys. vol. 313 (1–3), pp. 325-329.

[36] D. Feller, K.A. Peterson, and J. G. Hill: J. Chem. Phys., 2011, vol. 135 (4), 044102.

[37] J. Safarian, M. Tangstad: Metall. Mater. Trans. B, 2012, vol. 43B, pp. 1427-1445.